On the Pressure Gradient Force Error in σ-Coordinate Spectral Models

ZAVIŠA I. JANJIĆ

Institute for Meteorology, Faculty of Physics, University of Belgrade, Yugoslavia

16 August 1988 and 10 April 1989

ABSTRACT

The pressure gradient force error of the spectral technique used in combination with the σ vertical coordinate was examined in an idealized case of an atmosphere at rest and in hydrostatic equilibrium. Small-scale (one-point and three-point) mountains were used in the tests. With such definitions of topography, difficulties could be expected with the spectral method due to slow convergence of the Fourier series. For reference, the finite-difference pressure gradient force errors were also computed. In the examples considered, it was found that the errors of the spectral method can be large. In the rms sense, the spectral pressure gradient force errors were larger than those of the finite-difference method.

1. Introduction

The pressure gradient force errors in σ-coordinate spectral models are often believed to be small or unimportant, although little evidence has been published to support such a view. A general idea about the magnitude of these errors can be obtained from the paper by Simmons (1987).

The principal difficulty in assessing the significance of this, and other σ-coordinate problems (advection, horizontal diffusion) arises due to the fact that a competitive technique for representing mountains in spectral models is missing. In a finite-difference model, an alternative vertical coordinate with step-like representation of topography (Mesinger 1984) has been recently introduced and is currently being tested (Black and Janjić 1988; Janjić et al. 1988; Mesinger et al. 1988).

The purpose of the present exercise is to assess the order of magnitude of the pressure gradient force errors in σ-coordinate spectral models in the case of small-scale mountains, and to examine the spatial distribution of the errors. For reference, the errors of the finite-difference method will be also computed. An idealized atmosphere will be considered in the tests following the example of Mesinger (e.g., Mesinger and Janjić 1987). For simplicity, only the zonal component of the pressure gradient force will be discussed.

2. Experiment setup

Consider a horizontally homogenous atmosphere at rest, and in hydrostatic equilibrium. In such an atmosphere the pressure gradient force is zero everywhere, and the computed pressure gradient force in a discretized system will represent the error of the discretization method.

Let the following information about this atmosphere be available in a vertical cross section along a constant latitude:

(i) Surface pressure p_s (and therefore $\ln p_s$) on an equidistant horizontal grid with M independent points;

(ii) Surface geopotential Φ_s on the same M-point horizontal grid; and,

(iii) Geopotential Φ on the same M-point horizontal grid, and on L_m equidistant σ levels.

In addition, let the horizontal domain be scaled in such a way that the grid distance be equal to 1. Note that due to periodicity, for any function $f(i)$, where i is the horizontal index, $f(M+i)=f(i)$. The numerical values of M and L_m used in the calculations are 120 and 15, respectively.

Let us now consider the spectral horizontal representation in terms of trigonometric functions, which is equivalent to the grid-point representation on the M-point grid. The term "equivalent" is used here to denote the requirement that the spectral representation have the same number of degrees of freedom as the grid-point representation, and yield the same values at the grid points of the M-point grid. This requirement will be satisfied if the coefficients of the truncated trigonometric series are computed using the approximate Fourier transform formulae (e.g., Korn and Korn 1961).

In order to calculate the pressure gradient force error, spectrally represented temperatures on the σ levels are needed. Following e.g., Mesinger and Janjić (1987), the temperatures are retrieved from the geopotential.

Corresponding author address: Dr. Zaviša I. Janjić, Institute for Meteorology, University of Belgrade, Dobracina 16, P.O. Box 550, YU-11001 Belgrade, Yugoslvaia.

For this purpose we choose the hydrostatic equation introduced by Bourke (1974), which can be reformulated in the finite-difference form as

$$\Phi_L = \Phi_{L+1} + R[(T_{L+1} + T_L)/2] \ln(\sigma_{L+1}/\sigma_L), \quad \text{for} \quad L < L_m,$$

$$\Phi_{L_m} = \Phi_s + R\{T_{L_m} + [(T_{L_m} - T_{L_m-1})/\ln(\sigma_{L_m}/\sigma_{L_m-1})] \times \ln(1/\sigma_{L_m})/2\} \times \ln(1/\sigma_{L_m}). \quad (1)$$

Here, L_m is the lowest model level. The other symbols used have their usual meaning.

The spectrally represented temperatures can be obtained from the geopotentials using either of the following two procedures:

(i) Using (1), the grid point values of temperature are computed from the grid point values of geopotential, and then the temperature is converted into the spectral form; or

(ii) The geopotential is converted into the spectral form, and then the spectrally represented temperatures are obtained from the original, spectral form of Bourke's (1974) hydrostatic equation.

Due to linearity of the operators involved, both procedures yield the same answer, except for (rather small) accumulated round off errors.

Having defined the temperatures, the pressure gradient force error of the spectral method is calculated using the following procedure:

- The spectral coefficients of $\partial \ln p_s/\partial x$ are calculated, and then these coefficients are used to recalculate the grid-point values of $\partial \ln p_s/\partial x$ on a regular $2M$-point grid, i.e., the grid with twice the resolution of the original M-point grid.
- The spectral coefficients of $-\partial\Phi/\partial x$ are calculated from the spectrally represented geopotentials on each σ level, and then the coefficients of the expansion of $-\partial\Phi/\partial x$ are used to compute the grid-point values of $-\partial\Phi/\partial x$ on the M-point grid. This is the first term of the pressure gradient force.
- The spectral coefficients of temperature on each σ level are used to recalculate the temperatures at the grid points of the $2M$-point grid.
- The product $-RT\partial \ln p_s/\partial x$ is calculated at the grid points of the $2M$-point grid on each σ level. Then, the spectral coefficients of this product are calculated, but all spectral components that cannot be represented on the M-point grid are truncated in order to avoid aliasing. The remaining coefficients are used to recalculate the values of $-RT\partial \ln p_s/\partial x$ at the grid points of the M-point grid. This is the second term of the pressure gradient force.
- The sum of the first and the second term of the pressure gradient force is the pressure gradient force error at the grid points of the M-point grid.

The pressure gradient force error of the finite-difference method is calculated by the formula:

$$-\delta_x\Phi_\sigma - R\bar{T}^x\delta_x \ln p_s.$$

Here, the symbol δ_x, and the overbar with subscript x, denote the simplest two-point differencing and averaging operators applied in the zonal direction. The subscript σ indicates that the differencing is performed on a σ surface.

The geopotential on the σ levels is calculated analytically from a chosen continuous temperature profile $T(p)$. Actually, following Mesinger (1982), two vertical temperature profiles are considered. The temperature at 800 mb level is taken to be 0°C in both cases, and it varies linearly with $\ln p$, reaching, respectively, 10°C ("no-inversion case") and −10°C ("inversion case") at the 1000 mb level. Above 800 mb the two profiles coincide, decreasing linearly with the same lapse rate as in the no-inversion case below 800 mb. This situation is schematically shown in Fig. 1. Note that with the profiles chosen, the temperatures become unrealistically low at higher model levels. This, however, has no impact on the errors at the lower levels, and generally does not affect the validity of the results at this level of idealization.

In the main experiment, a single-grid-point mountain is located in the middle of the horizontal domain, i.e., at the point with the horizontal index $(M/2) + 1$. The remaining part of the domain is assumed to be flat. The surface pressure is set to 800 mb at the top of the mountain, and to 1000 mb over the flat terrain. This experiment setup is identical to that of Mesinger (e.g. Mesinger and Janjić 1987).

In order to examine the possible impact of the horizontal scale and the shape of the mountain, the experiments are repeated with three different shapes of the three-point mountain: a triangular mountain with the slopes linear in $\ln p$, an obelisk-shaped mountain, and a trapezoidal mountain (three-point elevated plateau). Note that the single-point mountain and the trapezoidal three-point mountain can be considered as extreme cases of the obelisk-shaped mountain. The tri-

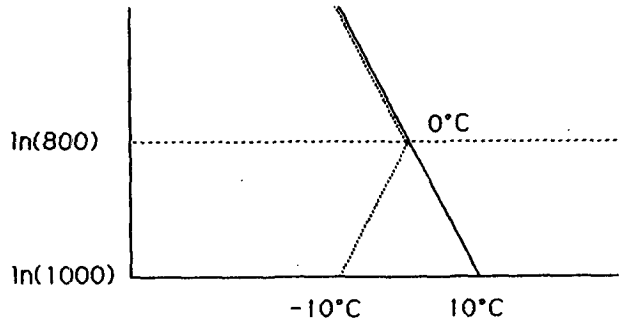

FIG. 1. Temperature profiles prescribed in the "inversion" (dotted) and "no-inversion" (solid) cases.

angular mountain can also be viewed as a special case of the obelisk-shaped mountain.

The surface pressures at the tops of the three-point mountains are again set to 800 mb. In the case of the obelisk-shaped mountain, the surface pressures at the two mountain points other than the top point are

$$p_s = [1000 - 200 \exp(-0.25)] \text{ mb} = 844.24 \text{ mb}.$$

The single-point mountain and the three-point mountains are shown schematically in Fig. 2. As indicated in the figure, with the currently used horizontal resolution, the widths at the bases of the single-point, and the three-point mountains are 6° and 12°, respectively. Note that the heights and the slopes of the mountains chosen are rather modest compared to the examples of topography given, e.g., by Mesinger and Collins (1987). Nevertheless, difficulties may be expected with the spectral technique due to slow convergence of the Fourier series in the case of orography restricted to only several grid points.

3. Results

As already pointed out, the temperatures used in the tests are retrieved using the hydrostatic equation (1) from the analytically calculated geopotentials. In the no inversion case this procedure results in hardly detectable errors. This comes as no surprise considering that the temperature profile is linear in $\ln p$, and that the same profile is assumed in (1) (cf. e.g. Mesinger and Janjić 1985). Thus, the small discrepancies observed can be explained by the round-off errors. However, in the vertical columns with inversion, two-grid-interval noise appears, with the amplitude of slightly less than 2°K. This can be attributed to the averaging of temperature in (1).

In contrast to the finite-difference pressure gradient force error which is restricted to the points over the sloping terrain, the error of the spectral representation is spread over the horizontal domain. For this reason, the rms error is a more convenient measure of the pressure gradient force error than the grid point values.

a. Single-point mountain

The spectral rms pressure gradient force errors on the σ levels are shown in Fig. 3 (lightly shaded bars). The upper panel corresponds to the inversion, and the lower panel to the no-inversion case. For comparison, the rms errors of the finite-difference method (cross-hatched bars) are also displayed. As can be seen from the figure, in the rms sense, the pressure gradient force errors of the spectral method are considerably larger

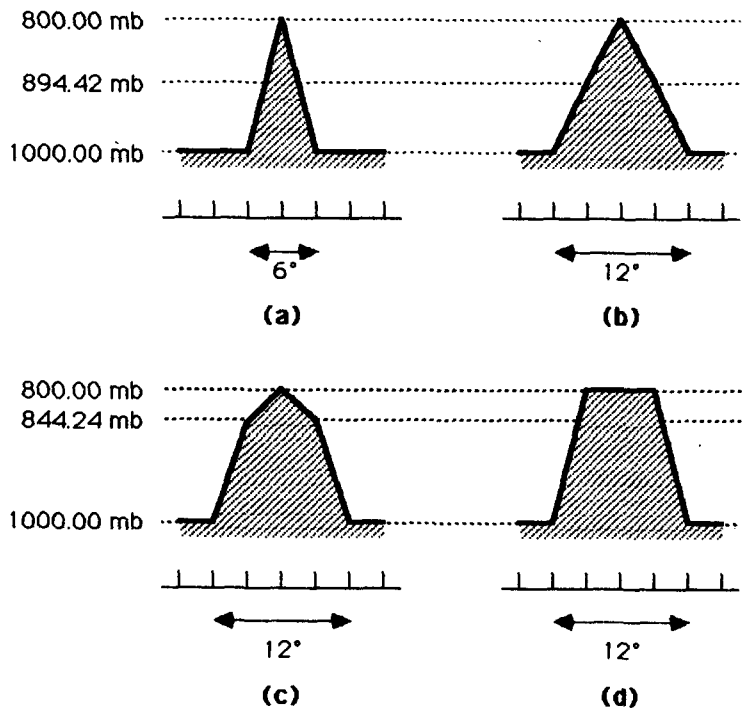

FIG. 2. Shapes of mountains used in the tests: (a) single-point mountain; (b) three-point triangular mountain with the slopes linear in $\ln p$; (c) three-point obelisk-shaped mountain; and (d) three-point trapezoidal (elevated plateau) mountain. The heights of the mountain points and the base widths of the mountains are also indicated.

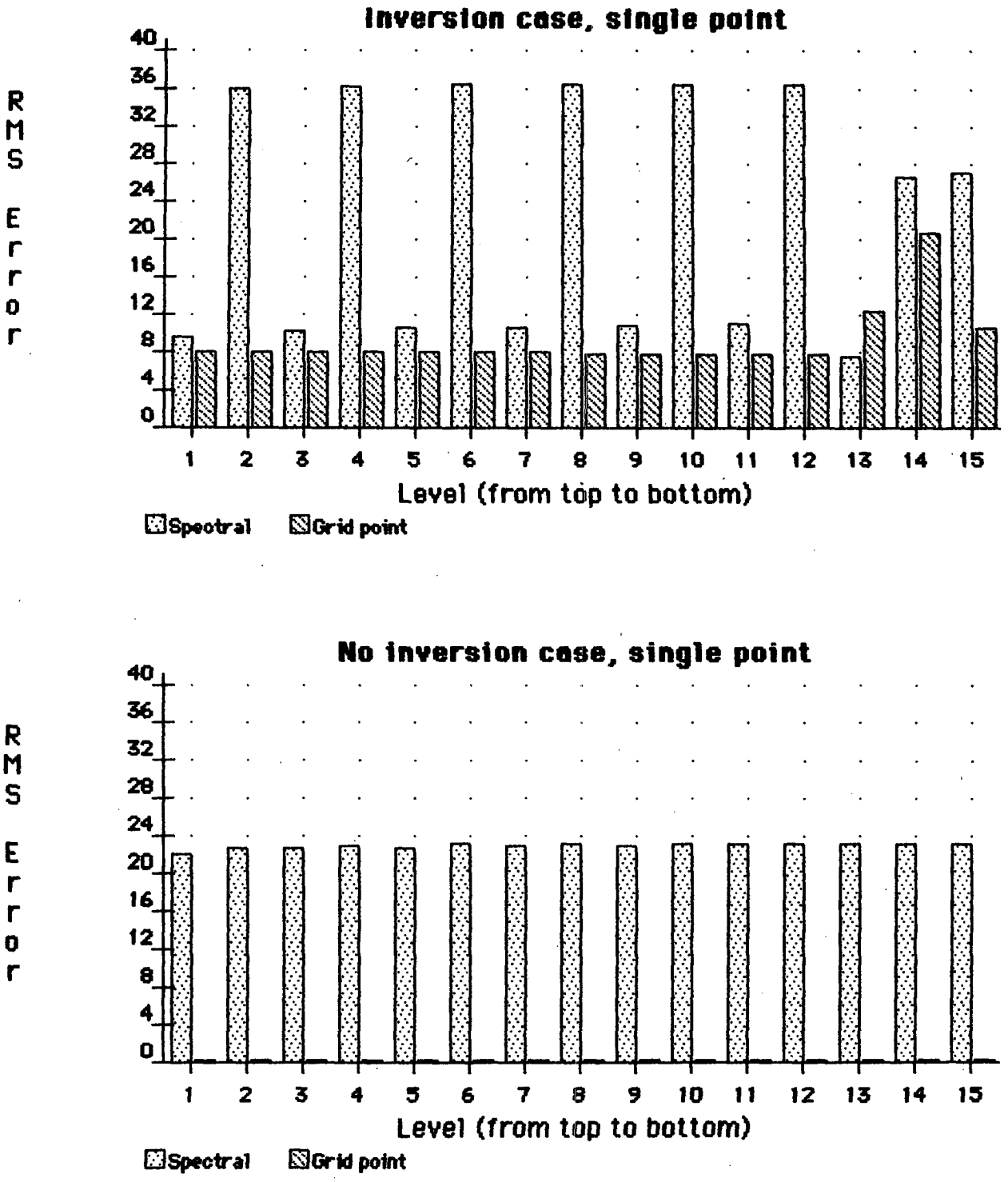

FIG. 3. The rms pressure gradient force errors corresponding to the single-grid point mountain for the inversion (upper panel) and no-inversion (lower panel) cases. The errors of the spectral and the finite-difference methods are represented by lightly shaded and cross-hatched bars, respectively. The plotted values are in units of geopotential.

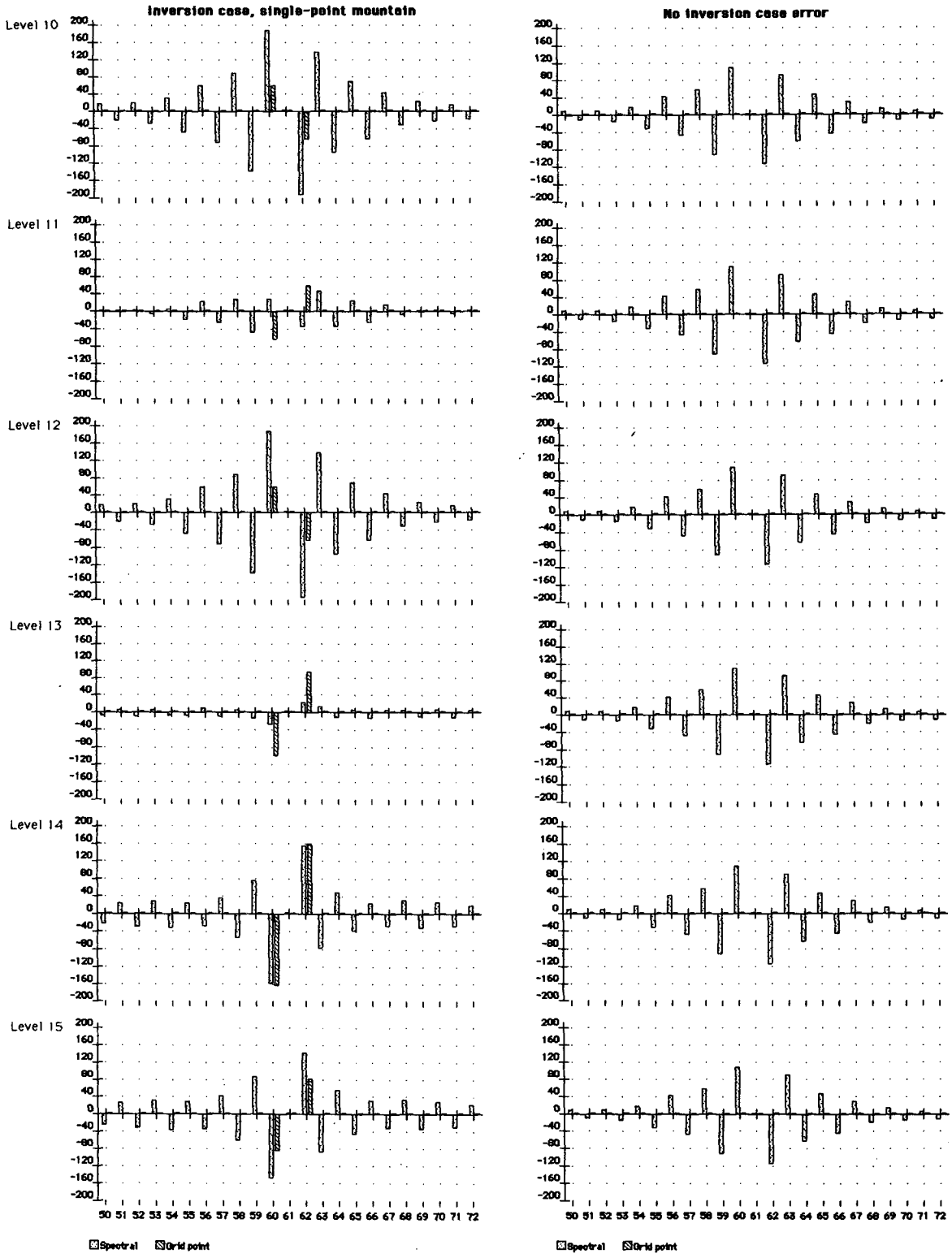

FIG. 4. Pressure gradient force error pattern around the mountain point at six lowest model levels for the spectral method (lightly shaded bars) and the finite-difference error (cross-hatched bars) for the inversion (left panel) and the no-inversion (right panel) cases. The finite-difference error bars are shifted for half a grid distance in the direction away from the mountain from the actual error locations. The ploted values are in units of geopotential.

than those of the finite-difference method, particularly in the no-inversion case; in this case, due to the temperature profile and the pressure gradient force scheme chosen, the errors of the finite-difference method are hardly detectable (cf. e.g. Mesinger and Janjić 1985).

In order to examine their spatial distribution, the pressure gradient force errors of the spectral method around the mountain point are plotted for the six lowest model levels in Fig. 4 (lightly shaded bars) for both inversion (left panel) and no-inversion (right panel) cases. Going further up, the error patterns of levels 11 and 10 very much repeat themselves, switching from one to the other, depending on whether the vertical index is even or odd. For comparison, the finite-difference pressure gradient force error is also displayed (cross-hatched bars) at the two points adjacent to the mountain point. It should be noted that the finite-difference errors are actually defined in between the mountain point and the two adjacent points. Thus, in the figure, they are shifted for half a grid distance away from their actual location.

Note that in the inversion case the amplitude of the spectral error wave packet is generally of the same order of magnitude as the errors of the finite-difference method. The large error of the spectral technique in the no-inversion case is somewhat surprising.

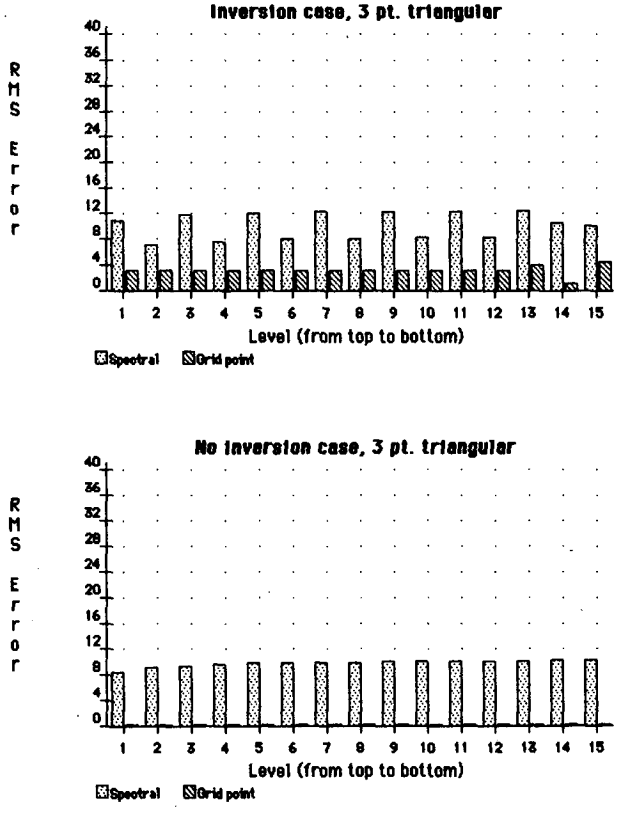

FIG. 5. Same as Fig. 3, but for the triangular three-point mountain.

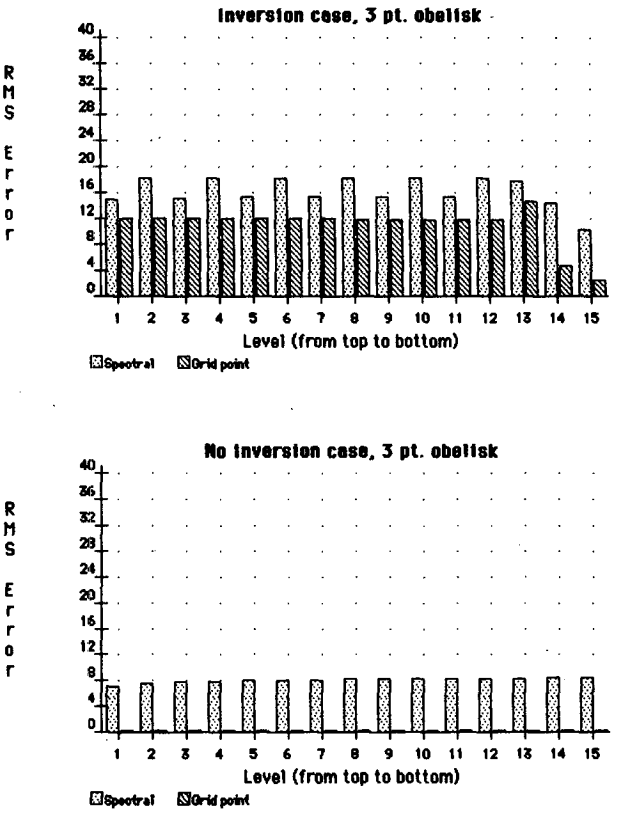

FIG. 6. Same as Fig. 5, but for the obelisk-shaped three-point mountain.

b. *Three-point mountains*

The rms pressure gradient force errors on the σ levels for the triangular, obelisk and trapezoidal shaped three-point mountains are shown in Figs. 5, 6 and 7, respectively. Again, the upper panels correspond to the inversion, and the lower ones to the no inversion cases. As before, the lightly shaded bars are reserved for the spectral, and the cross hatched bars for the finite-difference method.

As can be seen from Fig. 5, in the case of the triangular mountain, the rms errors are significantly reduced compared to the single-point mountain. However, in the rms sense, the pressure gradient force errors of the spectral method are again considerably larger. As expected, the errors of the finite-difference method in the no-inversion case are negligible.

Compared to the triangular mountain, the results for the obelisk-shaped mountain show a general increase of the rms errors in the inversion case. Note that the errors of the finite-difference method at higher levels are larger than those corresponding to the single-point mountain, and approach the errors of the spectral method. In the no-inversion case, the errors of the spectral method are slightly smaller than in the case of the triangular mountain.

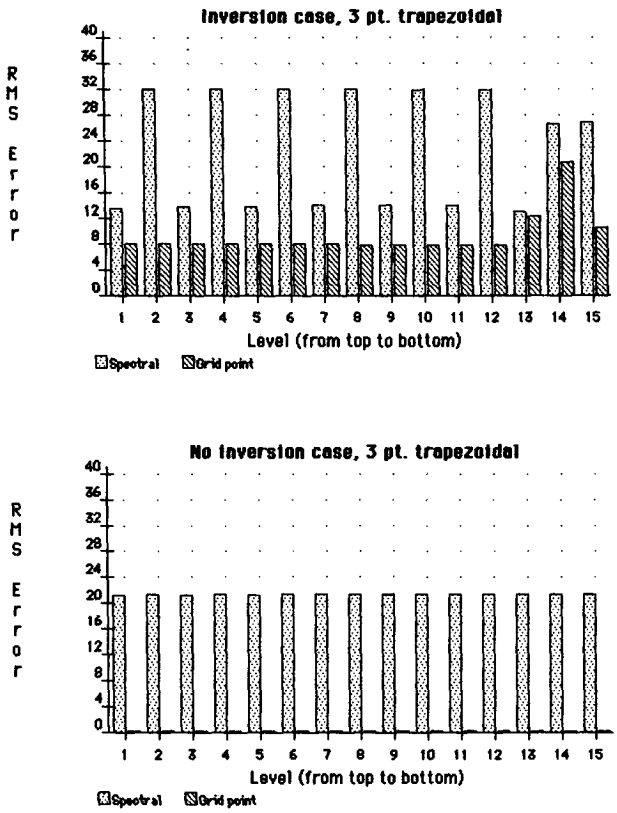

FIG. 7. Same as Fig. 6, but for the trapezoidal (elevated plateau) three-point mountain.

The errors for the trapezoidal mountain very much resemble those for the single-point mountain, except for the fact that the amplitude of two-grid-interval wave in the spectral rms error is now reduced.

In all tests with the three-point mountains, in the inversion case the amplitude of the spectral error wave packet (not shown) remained generally of the same order of magnitude as the errors of the finite-difference method.

4. Conclusions

The examples of small-scale mountains considered indicated that the σ-coordinate pressure gradient force errors of the spectral method can be large, and that the errors spread away from the mountains. In the rms sense, these errors were larger than the errors of the finite-difference method. In the inversion case, the amplitudes of the spectral error wave packets were generally of the same order of magnitude as the errors of the finite-difference method.

Contrary to the situation with the finite-difference method, the magnitude of the rms pressure gradient force error of the spectral method showed much less sensitivity to the absence of the inversion. Namely, the error of the latter remained relatively large, while the error of the former almost vanished.

The experiments with varying the horizontal scale and the shape of the mountain showed the sensitivity of the spectral method to the steepness of the mountain. Generally, the steeper the mountain, the larger the pressure gradient force error. However, in the no-inversion case, the rms errors of the generally steeper obelisk mountain were slightly smaller than those of the triangular mountain.

The pressure gradient force errors of the spectral method showed little sensitivity to changing from the single-point mountain to the trapezoidal three-point mountain. Note that the steepnesses of the slopes of these two mountains are the same. This suggests that the errors are less sensitive to the horizontal scale of the mountain than to its steepness.

Relatively large pressure gradient force errors of the spectral method observed in the no-inversion case indicate that the mechanisms responsible for the error are different from those of the finite-difference σ-coordinate models. Consequently, the methods for reducing the error in the finite-difference models (e.g. Gary 1973; Janjić 1977, 1980; Mesinger and Janjić 1985; Mihailović and Janjić 1986) should not be expected to operate effectively.

As already pointed out, it seems natural to expect difficulties with spectral representation in the presence of small-scale topography because of slow convergence of the Fourier series. In this situation, in order to calculate the pressure gradient force in σ-coordinate spectral models, it may be advantageous to use the finite-difference technique on the finer grid used to eliminate aliasing.

Acknowledgments. This research was supported by the Science Association of Serbia, Belgrade. The author is grateful to one of the reviewers for a suggestion that lead to the definition of the three-point obelisk-shaped mountain.

REFERENCES

Black, T. L., and Z. I. Janjić, 1988: Preliminary forecast results from a step-mountain eta coordinate regional model. *Eighth Conference on Numerical Weather Prediction,* Baltimore, Amer. Meteor. Soc., 442–447.

Bourke, W., 1974: A multi-level spectral model. I. Formulation and hemispheric integrations. *Mon. Wea. Rev.,* **102,** 687–701.

Gary, J. M., 1973: Estimate of truncation error in transformed coordinate, primitive equation atmospheric models. *J. Atmos. Sci.,* **30,** 223–233.

Janjić, Z. I., 1977: Pressure gradient force and advection scheme used for forecasting with steep and small scale topography. *Beitr. Phys. Atmos.,* **50,** 186–199.

——, 1980: Numerical problems related to steep mountains in sigma coordinates. *Workshop on Mountains and Numerical Weather Prediction,* 1979, ECMWF, Shinfield Park, Reading, U.K., 48–89.

——, F. Mesinger and T. L. Black, 1988: Horizontal discretization and forcing. *Workshop on Numerical Techniques for the Horizontal Discretization in Numerical Weather Prediction Models,* ECMWF, Shinfield Park, Reading, U.K., 207–227.

Korn, G. A., and T. M. Korn, 1961: *Mathematical Handbook for Scientists and Engineers.* McGraw-Hill (Russian translation) 720 pp.

Mesinger, F., 1982: On the convergence and error problems of the calculation of the pressure gradient force in sigma coordinate models. *Geophys. Astrophys. Fluid Dyn.,* **19,** 105–117.

——, 1984: A blocking technique for representation of mountains in atmospheric models. *Riv. Meteor. Aeronautica,* **44,** 195–202.

——, and W. G. Collins, 1987: Review of the representation of mountains in numerical weather prediction models. *Observation, Theory and Modelling of Orographic Effects, Vol. 2,* Seminar/workshop 1986, ECMWF, Shinfield Park, Reading, U.K., 1–28.

——, and Z. I. Janjić, 1985: Problems and numerical methods of the incorporation of mountains in atmospheric models. *Large-scale Computations in Fluid Mechanics, Part 2, Lect. Appl. Math., Vol. 22,* Amer. Math. Soc., 81–120.

——, and ——, 1987: Numerical techniques for the representation of mountains. *Observation, Theory and Modelling of Orographic Effects, Vol. 2,* Seminar/workshop 1986, ECMWF, Shinfield Park, Reading, U.K., 29–80.

——, ——, S. Ničković, D. Gavrilov and D. G. Deaven, 1988: The step-mountain coordinate: model description and performance for cases of Alpine lee cyclogenesis and for a case of an Appalachian redevelopment. *Mon. Wea. Rev.,* **116,** 1493–1518.

Mihailović, D. T., and Z. I. Janjić, 1986: Comparison of methods for reducing the error of the pressure gradient force in sigma coordinate models. *Meteor. Atmos. Phys.,* 177–184.

Simmons, A. J., 1987: Orography and the development of the ECMWF forecast model. *Observation, Theory and Modelling of Orographic Effects, Vol. 2,* Seminar/workshop 1986, ECMWF, Shinfield Park, Reading, U.K., 129–163.